Kinetic Control of Interpenetration in Fe-Biphenyl-4,4′-Dicarboxylate Metal-Organic Frameworks by Coordination and Oxidation Modulation

Dominic Bara,[1] Claire Wilson,[1] Max Mörtel,[2] Marat M. Khusniyarov,[2] Sanliang Ling,[3] Ben Slater,[4] Stephen Sproules,[1] Ross S. Forgan[1]*

1. WestCHEM School of Chemistry, University of Glasgow, Joseph Black Building, University Avenue, Glasgow G12 8QQ, UK.

2. Department of Chemistry and Pharmacy, Friedrich-Alexander University Erlangen-Nürnberg, Egerlandstrasse 1, 91058 Erlangen, Germany.

3. Advanced Materials Research Group, Faculty of Engineering, University of Nottingham, University Park, Nottingham NG7 2RD, UK.

4. Department of Chemistry, University College London, 20 Gordon Street, London, WC1H 0AJ, UK.

Email: Ross.Forgan@glasgow.ac.uk

Abstract

Phase control in the self-assembly of metal-organic frameworks (MOFs) is often a case of trial and error; judicious control over a number of synthetic variables is required to select the desired topology and control features such as interpenetration and defectivity. Herein, we present a comprehensive investigation of self-assembly in the Fe-biphenyl-4,4′-dicarboxylate system, demonstrating that coordination modulation can reliably tune between the kinetic product, non-interpenetrated MIL-88D(Fe), and the thermodynamic product, two-fold interpenetrated MIL-126(Fe). Density functional theory simulations reveal that correlated disorder of the terminal anions on the metal clusters results in hydrogen-bonding between adjacent nets in the interpenetrated phase and is the thermodynamic driving force for its formation. Coordination modulation slows self-assembly and therefore selects the thermodynamic product MIL-126(Fe), while offering fine control over defectivity, inducing mesoporosity, but electron microscopy shows MIL-88D(Fe) persists in many samples despite not being evident by diffraction. Interpenetration control is also demonstrated using the 2,2′-bipyridine-5,5′-dicarboxylate linker; it is energetically prohibitive for it to adopt the twisted conformation required to form the interpenetrated phase, although multiple alternative phases are identified due to additional coordination of Fe cations to its N-donors. Finally, we introduce oxidation modulation – the use of metal precursors in different oxidation states to that found in the final MOF – to kinetically control self-assembly. Combining coordination and oxidation modulation allows the synthesis of pristine MIL-126(Fe) with BET surface areas close to the predicted maximum for the first time, suggesting that combining the two may be a powerful methodology for the controlled self-assembly of high-valent MOFs.

1. Introduction

Metal-organic frameworks (MOFs) are comprised of metal ions or clusters linked by organic ligands into network structures, and have attracted a large amount of interest in recent years.[1-4] Their high porosities, combined with the ability to tune their structures and physical properties, makes them highly desirable for a number of applications, such as gas storage,[5-6] catalysis,[7] and sensing,[8-10] with MOFs prepared from low toxicity metals and ligands attractive in biomedical settings such as drug delivery.[11-12] MOFs constructed from Fe^{3+} cations (as well as other trivalent metals such as Cr^{3+}, Sc^{3+}, etc.) and dicarboxylate linkers often adopt structures in the MIL-88 (MIL stands for Materiaux Institut Lavoisier) series, where six-connected $[Fe_3O(RCO_2)_6(H_2O)_2X]$ (X = monoanion) secondary building units (SBUs) (Figure 1a) are linked into hexagonal nets by the ditopic linkers.[13] The iron MOF linked by biphenyl-4,4′-dicarboxylate (bpdc) is typically doubly interpenetrated (Figure 1b), giving a structure known as MIL-126(Fe).[14]

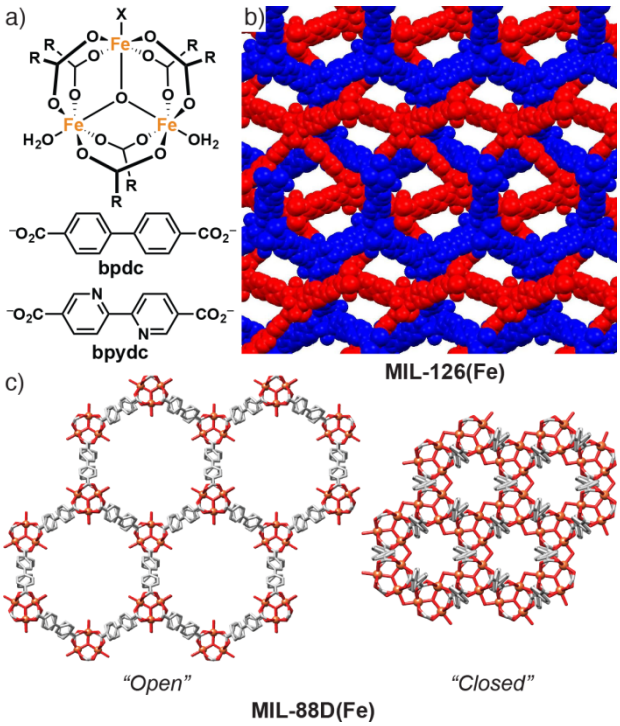

Figure 1. a) Structures of the $[Fe_3O(RCO_2)_6(H_2O)_2X]$ (X = monoanion) SBU and linear dicarboxylate linkers used in this study. b) Packing structure of the two-fold interpenetrated MIL-126(Fe), with the distinct nets coloured red and blue. Redrawn from CCDC deposition MIBMER.[14] c) Packing structures, viewed down the *c* axis, of open and closed MIL-88D(Fe), generated from simulated structures (not to scale),[15] C: grey; O: red; Fe: orange spheres; H atoms removed for clarity.

Interpenetration, where multiple MOF networks are interwoven, is a well-known phenomenon that leads to reduced pore volume and can enhance framework rigidity.[16] The non-interpenetrated analogue, MIL-88D (Figure 1c), has been isolated for Cr^{3+},[13] but the Fe^{3+} MOF has only been reported as a poorly crystalline product from low temperature syntheses that rapidly converted to the interpenetrated phase.[14] Established strategies for controlling interpenetration in MOFs include variation of synthetic parameters[17], choice of solvent[18], and increasing the steric bulk of the linkers[19]. In the case of MIL-126(Fe), the two-fold interpenetration restricts the flexibility of the nets and thus confers rigidity and permanent porosity to the MOF, in contrast to MIL-88D materials which, along with other non-interpenetrated analogues in the isoreticular series, collapse to a closed pore form on desolvation and are typically non-porous.[20] The permanent porosity and distribution of Lewis acid sites in MIL-126(Fe) has resulted in its application as a heterogeneous catalyst.[21-25]

For bioapplications, the ability to control particle size is necessary to avoid accumulation of the MOF in the bloodstream and ensure their effective uptake into the targeted cells.[26] Coordination modulation, the addition of monotopic linkers to MOF syntheses, is one established synthetic tool for tuning the crystal size of MOFs.[27-32] Competition between the modulator and the linker can slow the crystallisation, leading to larger and less polydisperse crystallites as well as enhancing crystallinity,[33] but under certain conditions the modulator can act as a capping agent and generate surface-modified nanoparticles. Modulation is typically effective in the synthesis of MOFs linked by high valent metal cations such as Zr^{4+}, which act as hard acids, giving rise to more kinetically inert metal-ligand bonds that are more resilient to hydrolysis and substitution but prone to forming amorphous or poorly crystalline materials.[34-35] Fe based MOFs have attracted particular interest for drug delivery due to their relative stability and the endogenous nature of iron,[36-37] an advantage over many of the metals commonly used in MOF synthesis.

We have previously shown that the synthesis of MIL-126(Sc) is highly amenable to modulation, controlling physical properties such as porosity and particle size, while substituting the bpdc linker for 2,2′-bipyridine-5,5′-dicarboxylic acid (bpydc) allows effective control of interpenetration through the conformation of the linker.[38] Reported examples of coordination modulation applied to iron MOFs, however, are relatively scarce,[39-44] but it has been combined with the use of pre-formed $[Fe_3O(OAc)_6(H_2O)_2(OH)]$ clusters to give single crystals of a number of systems.[45] Herein we present an extensive study into coordination

modulation of iron MOFs linked by bpdc and bpydc, investigating the effect of tuning synthetic parameters on interpenetration, porosity, defectivity, and particle size.

2. Synthesis of Fe-bpdc MOFs (1)

Preliminary solvothermal syntheses were carried out using $FeCl_3 \cdot 6H_2O$ and H_2bpdc as starting materials, both with and without the addition of a modulator (SI, Section S2). Based on our previous modulated synthesis of the interpenetrated scandium analogue MIL-126(Sc),[38] similar syntheses in *N*,*N*-dimethylformamide (DMF) at 120 °C using acetic acid (AA) as the modulator was attempted. After allowing to cool down to room temperature, the materials were centrifuged and washed three times with fresh DMF, followed by three washes with dichloromethane (DCM), before drying under vacuum at room temperature. The unmodulated and modulated samples were named **1** and **1-AA**, respectively. Highly crystalline material was obtained when 10 equivalents of acetic acid were added to the synthesis, with the powder X-ray diffraction (PXRD) pattern for **1-AA** matching the predicted PXRD pattern for MIL-126(Fe). In the absence of modulator, a poorly crystalline material, **1**, was obtained which possessed distinctly different diffraction peaks, indicating a different crystal phase (Figure 2a). Comparison with the simulated structure of MIL-88D(Fe) in the closed form[15] suggests that the unmodulated sample adopts this non-interpenetrated structure, although the poor crystallinity of **1** makes identification from PXRD alone less than conclusive. Imaging the samples with scanning electron microscopy (SEM) shows **1** consists of crystals with a rod-like morphology similar to those reported for the rest of the MIL-88 series,[39, 46] while **1-AA** contains larger intergrown crystallites (Figure 2b).

To confirm that **1** is the non-interpenetrated material, N_2 adsorption isotherms were performed at 77 K after activation at 150 °C for 20 hours under vacuum (Figure 2c). Upon removal of solvent molecules, MOFs in the MIL-88 series assume a state where their pores are closed and cannot be probed using gas sorption experiments. In contrast, the rigidity of interpenetrated MIL-126(Fe) allows it to be activated without a significant change in pore size, enabling these materials to adsorb nitrogen gas (reported surface areas of 1690-1750 m^2g^{-1}).[14, 15, 47] As expected, **1** had a much lower nitrogen uptake than **1-AA**, indicating that the unmodulated sample adopts the low porosity closed conformation characteristic of non-

interpenetrated MIL-88D. Interestingly, the isotherm for **1-AA** exhibits Type IV mesoporosity, suggestive of a defective material, with S_{BET} = 879 m^2g^{-1}.

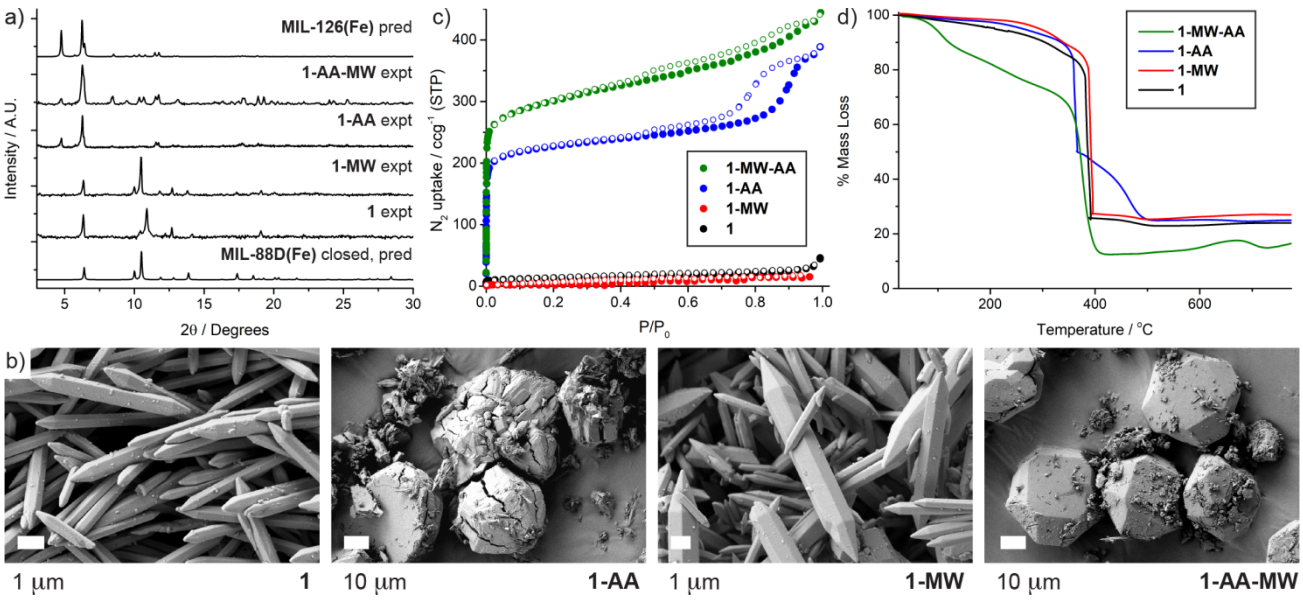

Figure 2. a) Stacked PXRD patterns of samples of 1 compared to predicted patterns for MIL-88D(Fe) in the closed state and MIL-126(Fe). b) SEM images of the samples of **1** showing morphology differences resulting from modulation. c) N_2 uptake isotherms (77 K) for the samples of **1** (filled symbols indicate adsorption, empty symbols desorption) Interpenetration is indicated by porosity. d) Thermogravimetric analyses of the samples of **1**.

Despite the structural differences between the interpenetrated and non-interpenetrated MOFs, they have the same overall framework formula $[Fe_3O(bpdc)_3(H_2O)_2X]$ and are expected to exhibit similar thermal properties. Thermogravimetric analysis (TGA) in air was performed on both samples to assess their thermal stabilities and estimate their approximate compositions (Figure 2d). Each sample had a steep mass loss at around 350 °C corresponding to framework degradation. The degradation of **1** occurs at a slightly higher (~10 °C) temperature than the modulated sample, again suggesting a different phase. The mass residues are consistent with the expected formula, however, the mass residue for **1-AA** does not indicate significant defectivity, despite its clear mesoporosity. This suggests that this defectivity is in the form of both missing-linkers and missing-clusters, which have opposing influence on the mass of the residue.

We propose that modulation slows the self-assembly process by competition with the linker to yield MIL-126(Fe) as the thermodynamic product, while the unmodulated synthesis yields MIL-88D(Fe) as the kinetic product. This would also explain why MIL-88D(Cr) is the predominant product of related syntheses, as Cr(III) is considerably more kinetically inert.[48]

Owing to the poor crystallinity of **1** prepared under solvothermal heating, an analogous synthesis using microwave heating was attempted, with rapid microwave heating expected to induce fast nucleation of the kinetic MIL-88D(Fe) phase; crystalline material was obtained within 5 minutes. The heating parameters were varied to optimise the synthetic conditions (See SI, Section S2), with the resulting materials assessed by PXRD and SEM analysis. Syntheses at both 100 and 120 °C yield the non-interpenetrated phase, with the lower temperature synthesis giving the highest intensity diffraction peaks, while at 150 °C the interpenetrated phase can be seen. The optimum conditions to obtain the non-interpenetrated material were 100 °C and 30 minutes (named **1-MW**); comparison with **1** shows that **1-MW** has a higher crystallinity and the diffraction peaks are in much better agreement with the predicted PXRD pattern for the closed conformation of MIL-88D(Fe) (Figure 2a). Additionally, as-synthesised, undried **1-MW** exhibits a PXRD pattern that closely mirrors the predicted structure for the open form of MIL-88D(Fe), confirming its flexibility (See SI, Figure S3). The formation of MIL-126(Fe) at higher temperatures under microwave heating again suggests it is the thermodynamic product.

A similar microwave synthesis using 10 equivalents of AA was also attempted. Crystalline material (**1-AA-MW**) was obtained at 120 °C after 30 minutes, corresponding to the interpenetrated MIL-126(Fe) phase. The PXRD patterns of **1-MW** and **1-AA-MW** were indexed and the unit cell parameters were extracted by Pawley fitting using the program GSAS-II.[49] Close matches with the crystallographic data predicted for MIL-88D(Fe) and Mil-126(Fe) were observed for **1-MW** and **1 -AA-MW**, respectively (See SI, Figures S6 and S7). SEM imaging revealed that this sample consists mainly of well-faceted single crystals of around 30 μm in diameter, while **1-MW** shows the hexagonal rod morphology characteristic of MIL-88D (Figure 2b). **1-MW** and **1-AA-MW** display similar thermal stability and porosity to the solvothermal analogues (Figures 2c and 2d), confirming effective interpenetration control through coordination modulation.

3. DFT Investigation of Thermodynamic Factors

To investigate the influence of thermodynamic factors for MIL-126 and MIL-88D topologies, first-principles calculations have been undertaken on the pristine frameworks (SI, Section S3) of the experimentally studied Fe-based material and the Sc analogues of these phases.[38] The $[M_3O(RCO_2)_6(H_2O)_2X]$ SBU in both frameworks contains three metal ions that are capped with one anion (X, presumed to be OH^-) and two water molecules. In the MIL-88D topology, the positioning of the anion and water ligands does not influence the internal energy of the framework significantly, as all the configurations explored in this work fall within a ~1 kJ mol^{-1} window (~1 kJ mol^{-1} for the Sc analogue), which is comparable to kT at room temperature, indicating random positioning of the anions over the structure. Intriguingly however, for MIL-126, the situation is radically different. Tight two-fold interpenetration results in a close contact between the two nets at four points per unit cell, and the capping ligands can interact at these pinch points. A hydroxide anion on one sub-lattice entering into a H-bond with a water ligand on the other is strongly preferred by 33 kJ mol^{-1} (55 kJ mol^{-1} for the Sc analogue) over a close anion-anion interaction and some 48 kJ mol^{-1} (66 kJ mol^{-1} for the Sc analogue) over a water-water interaction (Figure 3). The energy scale for positioning the capping species in MIL-126 is a factor of 30 times larger than for MIL-88D and >~13 kT at room temperature, indicating that these thermodynamic factors are important in attaining the most stable arrangement of MIL-126 – confirming it is the thermodynamic product compared to the kinetic product MIL-88D – in line with what was observed experimentally. This enhanced probability of anion ordering could also be termed correlated disorder[50] and we speculate that it could be present in other MOFs where related clusters come into close contact with each other.

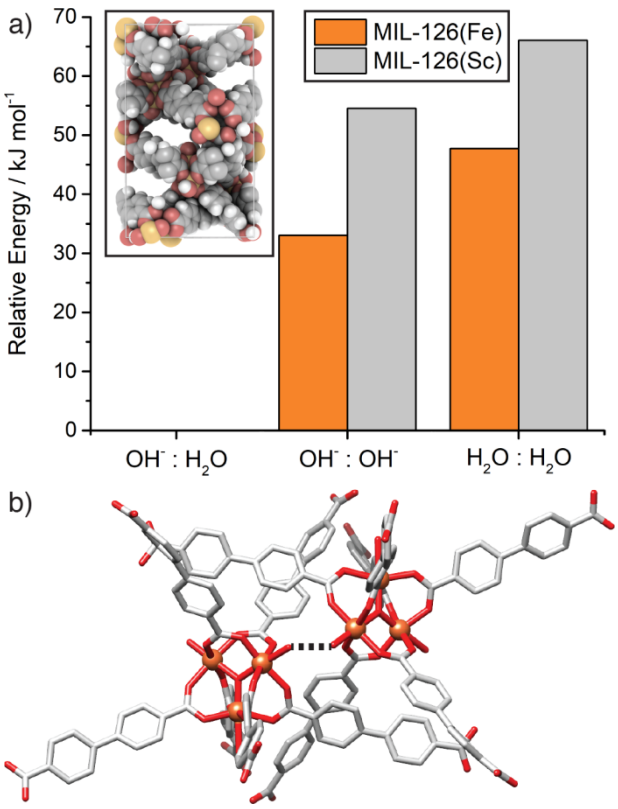

Figure 3. a) Relative energies of different arrangement of capping species between the sub-lattices in MIL-126 for both Fe and Sc analogues. Inset is a figure of the MIL-126(Fe) unit cell (Fe orange, oxygen red, carbon grey, hydrogen white) showing close interpenetration of the sub-lattices. b) Image of one of the four close points or "pinch-points" between the sub-lattices of MIL-126(Fe) which favours correlated disorder through anion-water ordering in this structure. Note that for the single MIL-88D lattices, permuting the anion and water positions changes the internal energy by only 1 kJ mol^{-1}, hence no such correlated disorder is expected in MIL-88D. C: grey; O: red; Fe: orange spheres.

4. Modulation of 1

With modulation control over interpenetration of **1** demonstrated using acetic acid, a range of different modulators, and their effect on the crystallinity, crystal size, and defectivity of **1**, were investigated (SI, Section S4). Samples were named "**1-mod** (x eq)" where mod is the modulator used and x = the number of equivalents of modulator added to the synthesis with respect to Fe.

4.1 Acetic Acid (AA). Following our initial results, studies were firstly focussed on acetic acid (AA); crystalline material was obtained from syntheses containing 1-20 equivalents of AA, above which no solid material formed. Five or more equivalents are required to obtain a highly crystalline material, indicating that the modulator plays a vital role in aiding crystallisation of the interpenetrated phase. Above 5 equivalents, no significant difference in crystallinity can be seen from the PXRD patterns, however there is a marked decrease in yield and changes in the physical properties of the resulting samples. The porosity of the samples increases with increasing AA concentration (Figure 4a), although no samples reach the porosity expected of a pure MIL-126(Fe) phase, predicted to be 2550 m^2g^{-1}[114]; **1-AA** (20 eq) has the highest BET surface area of 1289 m^2g^{-1}. Hysteresis loops consistent with mesoporosity are present in the N_2 uptake isotherms of samples prepared with 5-20 equivalents of AA. This could be attributed to induced defects from acetates coordinating to the clusters, leading to missing linkers and/or clusters from the framework, thus enhancing porosity without compromising stability. Ordered acetate capping of $[Fe_3O(RCO_2)_6(H_2O)_2X]$ SBUs has previously been observed as a consequence of steric clashes between ligands in PCN-236, forming a monocapped, 5-connected cluster, and because of linker rigidity in PCN-264, forming a bicapped, 4-connected cluster.[45]

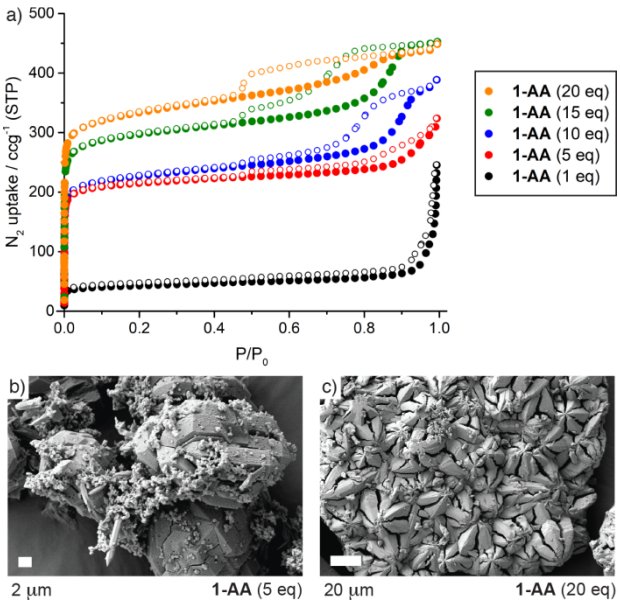

Figure 4. a) N_2 uptake isotherms (77 K, filled symbol adsorption, empty desorption) of samples of **1-AA** prepared with different quantities of AA. SEM images of b) **1-AA** (5eq) showing the presence of large intergrown blocks of MIL-126(Fe) alongside hexagonal needles of MIL-88D(Fe), and c) **1-AA** (20 eq) showing only intergrown sheets of MIL-126(Fe).

The pore size distributions show that all **1-AA** samples have the expected micropore at around 11 Å, as well as a mesopore at around 40 Å. TGA revealed a significantly lower oxide residue for **1-AA** (20 eq) than for the other samples, suggesting that as the quantity of modulator added to synthesis increases, missing clusters defects may become more prevalent compared to missing linker defects.

SEM imaging shows that **1-AA** (1 eq) consists mainly of broken rods, along with some larger block-like crystallites. Based on the morphology of the unmodulated samples, it is likely that these rods represent the non-interpenetrated MIL-88D(Fe) phase. Their broken, poorly defined nature is consistent with low crystallinity and would possibly explain why they are not evident in the PXRD pattern of the sample. In addition, their identification as MIL-88D(Fe) would explain the low porosity of the sample. Similar rod-like crystals, alongside much larger intergrown blocks, can also be seen in SEM images of **1-AA** (5 eq) (Figure 4b), again suggesting a mixed phase, but **1-AA** (20 eq) (Figure 4c) shows only large intergrown sheets which we assume represent MIL-126(Fe).

Subsequently, a range of modulators containing carboxylic acid groups, which can compete with the bpdc linker, and differ in their pK_a and steric bulk, was investigated, as they have been successfully used to modulate Zr MOFs.[10, 33, 51-54] The relative pK_a values of the modulators are expected to correlate with their binding strength to the SBUs and therefore potentially tune the degree of defectivity through their incorporation into the framework. Additionally, to independently study the effect of varying the pH of the reaction mixture, hydrochloric acid was also used as a modulator. The results are summarised in Figure 5.

In all cases, an optimum quantity of modulator to be added to the synthesis dictates a balance of crystallinity, yield, and porosity; in general, porosity increases with modulation (Figure 5a) but yields drop significantly (Figure 5b). Modulation produces predominantly MIL-126(Fe), but at lower modulator concentrations, the presence of MIL-88D(Fe) is evident in the form of rod-shaped crystals in SEM images while not being distinct in PXRD analysis. Modulation also results in a variety of particle morphologies of MIL-126(Fe) (Figure 5c). Carboxylate containing modulators tend to induce defects and mesoporosity, with the effect only minor for formic acid, while HCl modulation seems to produce MIL-126(Fe) material of the highest quality based on porosity analysis.

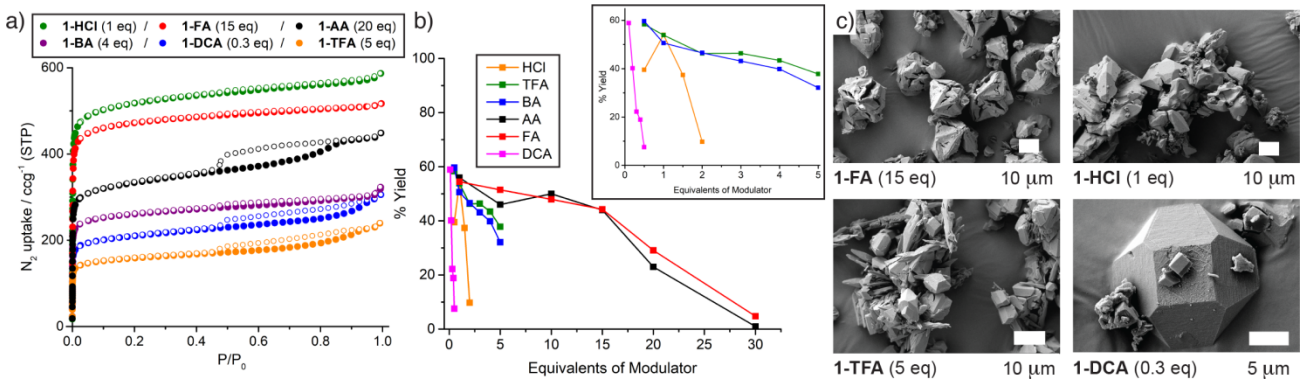

Figure 5. a) N_2 uptake isotherms (77 K, filled symbol adsorption, empty desorption) of optimal samples of **1** prepared with each modulator. b) Plot of reaction yields against modulator equivalents for each synthetic system, showing decrease in yield as more modulator is added. c) SEM images showing differing morphologies obtained with different modulators.

It is important to note that PXRD alone is not enough to assess phase purity; the presence of quantities of MIL-88D(Fe) in samples can be determined by SEM, and may account for the lower than predicted porosities of MIL-126(Fe) samples reported in the literature to date. Optimised conditions for each modulator based on the above parameters are detailed in Table 1.

Table 1. Optimum synthetic conditions (based on porosity) for MIL-126(Fe) with different modulators.

MOF	Mod Equiv	% Yield	BET Surface Area
1-AA	20	23%	1289 m^2g^{-1}
1-FA	15	44%	1871 m^2g^{-1}
1-BA	4	40%	1019 m^2g^{-1}
1-DCA	0.3	22%	808 m^2g^{-1}
1-TFA	5	38%	612 m^2g^{-1}
1-HCl	1	54%	2039 m^2g^{-1}

4.2 Formic Acid (FA). Highly crystalline material corresponding to MIL-126(Fe) could be obtained with one or more equivalent of FA, with an increasing amount of modulator giving a

similar reduction in yield as seen with AA. The N_2 uptake also increases with the addition of more modulator, but in contrast to AA, samples prepared with FA do not exhibit significant mesoporosity, indicating that the degree of defectivity in these samples is lower. Additionally, the approximate linker:cluster ratios based on TGA are generally close to the ideal value, which suggests that these samples contain approximately 3 linkers per cluster and are not significantly defective. Nitrogen adsorption isotherms show that the highest uptake is obtained with **1-FA** (15 eq), with a corresponding S_{BET} = 1871 m^2 g^{-1} slightly higher than the previously reported value of 1750 m^2 g^{-1}, but still lower than the value of 2550 m^2 g^{-1} predicted for an ideal material.[14] SEM imaging shows that **1-FA** (20 eq) has a distinctly different morphology which consists of spherical arrangements of smaller fused sheets rather than the more block-like crystals apparent in the other samples. The lower uptake could be a direct result of this morphology, which may reduce the pore continuity, making some of the pores inaccessible to nitrogen diffusion. Aside from this sample, the rest consist mostly of well-defined and regular single-crystals, which increase in size from around 10 µm to 40 µm as the modulator concentration is increased, with **1-FA** (30 eq) giving perfectly faceted single crystals but in very low yield. As with AA modulation, some additional rod-like crystals can be seen in the samples prepared with 1-10 equivalents of FA, again suggesting some non-interpenetrated MIL-88D(Fe) is present at lower modulator concentrations.

4.3 Dichloroacetic Acid (DCA). The use of dichloroacetic acid (DCA) as a modulator for Zr MOF syntheses can lead to its significant incorporation at defect sites, allowing it to be used as an effective probe molecule for endocytosis and anticancer drug delivery applications.[55-56] The crystallinity of the Fe materials increases with the quantity of DCA up until 0.5 equivalents, at which point it inhibits MOF formation; addition of one equivalent results in no solids formed. MIL-88D(Fe) appears to be present in **1-DCA** (0.05 eq) when imaged by SEM, as it consists mainly of hexagonal rods. Similar rods are present in samples modulated with up to 0.3 eq, alongside up to 30 µm, well-faceted crystals of MIL-126(Fe). The nitrogen uptake increases as the concentration of modulator increases, and there is also an increase in the hysteresis height, indicating the induction of defects, but porosity is considerably lower than expected, with the highest S_{BET} = 808 m^2 g^{-1} for **1-DCA** (0.3 eq).

4.4 Trifluoroacetic Acid (TFA). The low pK_a of TFA (0.23 compared to 4.76 for AA) was expected to lead to more defective samples, as has been reported for UiO-66.[53] PXRD indicates that the interpenetrated MOF can be prepared with addition of 0.5-5 equivalents of

TFA, but SEM revealed a significant proportion of hexagonal rods corresponding to MIL-88D(Fe) in all samples. Furthermore, the porosities are relatively low, with a maximum S_{BET} = 612 m^2 g^{-1} for **1-TFA** (5 eq), suggesting TFA is a poor modulator for this system.

4.5 Benzoic Acid (BA). Despite BA having a comparable pK_a to AA, syntheses using 10 or more equivalents yielded clear solutions with no solid product, whereas 30 equivalents of AA could be used and still result in crystallisation. Three equivalents of BA were required to crystallise MIL-126(Fe), with PXRD and SEM showing that fewer equivalents give MIL-88D(Fe). The use of 4 or 5 equivalents gave crystalline sheets, as was seen for higher concentration of AA, and **1-BA** (4 eq) possessed the highest porosity with S_{BET} = 1019 m^2 g^{-1}.

4.6 L-Proline. We have previously demonstrated L-proline to be an effective modulator for the synthesis of zirconium and hafnium MOFs[57] and also to obtain highly crystalline MIL-126(Sc).[38] Crystalline material matching the interpenetrated phase could only be obtained on addition of one equivalent to syntheses, above which only amorphous products were obtained, and all solids had a green colour. As L-proline has two coordination sites (both the amine and carboxylate) it is likely that its addition to syntheses containing the softer Fe^{3+} cation leads to the formation of a coordination polymer bridged by bidentate L-proline, which also explains the difference in colour for these samples. As such, it was not investigated further.

4.7 Hydrochloric Acid. It is assumed that the addition of monocarboxylates to MOF syntheses slows the crystallisation by competition with the linker for coordination sites, potentially pre-forming SBUs, and by lowering the pH.[58] Addition of a strong Brønsted acid should slow the self-assembly by hindering deprotonation of the linkers; to aid our understanding of this effect, concentrated hydrochloric acid (HCl), which has been shown to successfully enhance the synthesis of UiO-66 series MOFs,[59] was used. A clear increase in both the crystallinity and porosity of the interpenetrated MIL-126(Fe) phase that is formed can be observed as more HCl is added to the synthesis. The TGA trace for **1-HCl** (0.5 eq) shows an abnormally high oxide residue, suggesting that the sample consists of a disproportionate amount of inorganic material, likely iron oxides/hydroxides formed from reaction with the water present in HCl. When 2 equivalents of HCl are used, the crystallinity is very low, suggesting that there is an ideal pH range for successful crystallisation of the

MOF. The nitrogen adsorption isotherms of the MOFs all display Type I behaviour, typical for microporous materials, and do not display any hysteresis, suggesting minimal defectivity. While the chloride ion can act as the coordinating counterion to the Fe_3O cluster, it does not possess suitable coordinating groups to allow competition with the linker, therefore it is not expected to induce missing linker defects. **1-HCl** (1 eq) possesses the highest nitrogen uptake of all the samples presented so far, with for S_{BET} = 2039 m^2g^{-1}. There is also a large increase in crystal size as the concentration of HCl is increased, going from around 5-10 μm for **1-HCl** (0.5 eq) to around 100 μm for **1-HCl** (1.5 eq), indicating that HCl acts as an effective modulator.

5. Synthesis of Fe-bpydc MOFs (2)

The intermolecular interactions between the individual nets in interpenetrated structures, in this case H-bonding between capping ligands on the SBU, are important structure-directing forces which can drive interpenetration. Within the tightly interpenetrated MIL-126 framework, π-stacking between the bpdc linkers of the individual nets is evident, enabled by the twisted conformation adopted by bpdc to meet the steric constraints of the arrangement. Using Sc^{3+} as the metal, we have previously shown that replacing bpdc with 2,2′-bipyridine-5,5′-dicarboxylate (bpydc), which preferentially adopts a planar conformation, makes interpenetration less energetically favourable and results in a non-interpenetrated MIL-88D phase.[38] New DFT calculations (see SI, Section S3) suggest that a hypothetical MIL-126(Fe) form incorporating bpydc is highly destabilised due to the distortions of the bypdc linker, such that only 30 kJ mol^{-1} per sub-lattice is gained on interpenetrating two MIL-88D sub-lattices, whilst for bpdc, 92 kJ mol^{-1} per sub-lattice is liberated on interpenetrating two MIL-88D sub-lattices indicating a much stronger thermodynamic driving force to form the MIL-126(Fe) topology for the more flexible bpdc linker. These calculations correlate with our previous crystallographic database mining, which confirms that bpydc preferentially adopts a planar conformation in the solid-state.[38] To examine the analogous Fe^{3+}-bpydc system, solvothermal synthesis was performed at 120 °C both with and without use of a modulator (SI, Section S5). The samples are denoted **2** and "**2-mod** (x equiv)", respectively. PXRD patterns of the modulated samples show phases which correspond to the simulated PXRD patterns for MIL-88D(Fe), in contrast to the Fe^{3+}-bpdc system, however, in some cases there are additional phases which match neither the PXRD patterns for MIL-88D(Fe) or MIL-

126(Fe) (*vide infra*). The most successful synthesis of the MIL-88D phase was achieved with 2 equivalents of HCl (**2-HCl**), with PXRD showing relatively high crystallinity (Figure 6a) and well-formed hexagonal rods observed by SEM (Figure 6b).

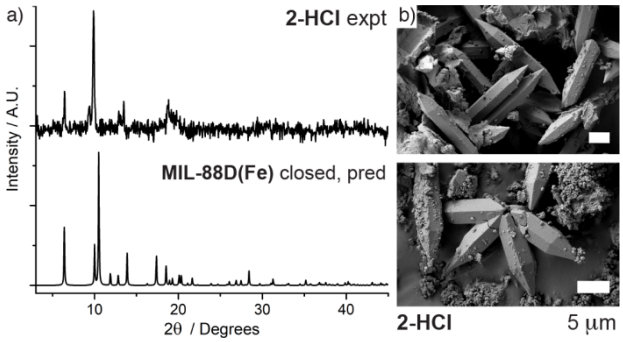

Figure 6. a) Stacked PXRD patterns of **2**-HCl compared to that predicted for MIL-88D(Fe) in the closed form. b) SEM images of **2**-HCl showing hexagonal rods characteristic of MIL-88D(Fe).

Attempts were made to obtain single crystals of Fe-bpydc to confirm the MIL-88D structure, following a procedure similar to recent work by Zhou *et al.* which uses pre-formed Fe-oxo-clusters and acetic acid to regulate the crystal growth (SI, Section S6).[45] As per the literature procedure, the synthesis was conducted in DMF at 150 °C for 18 h with the quantity of AA varied to obtain single crystals suitable for single-crystal X-ray diffraction. Syntheses resulted in two distinct crystal forms which could not be separated, named **3** and **4** respectively, which did not correspond to either MIL-126 or MIL-88D topologies. **3** crystallises as green plates (Figure 7a) in the tetragonal $P4_32_12$ space group, with linear trinuclear SBUs (Figure 7b) containing two crystallographically independent iron atoms (Fe1 and Fe2, related by a 2-fold rotation axis through the central Fe 1) both of which adopt six-coordinated distorted octahedral geometries. The central iron atom (Fe2) is coordinated to four oxygen atoms from four different bpydc linkers equatorial to the SBU, two each bridging to each Fe1 in the (η1:η1:μ2) motif, with two μ_2-oxo bridges at axial positions also bridging to each Fe1. The second iron atom (Fe1) is therefore coordinated by two oxygens from two different bpydc linkers, one μ_2-oxo bridge, one oxygen from a disordered monodentate formate/acetate ligand and terminated by two nitrogen donors from a single bpydc linker.

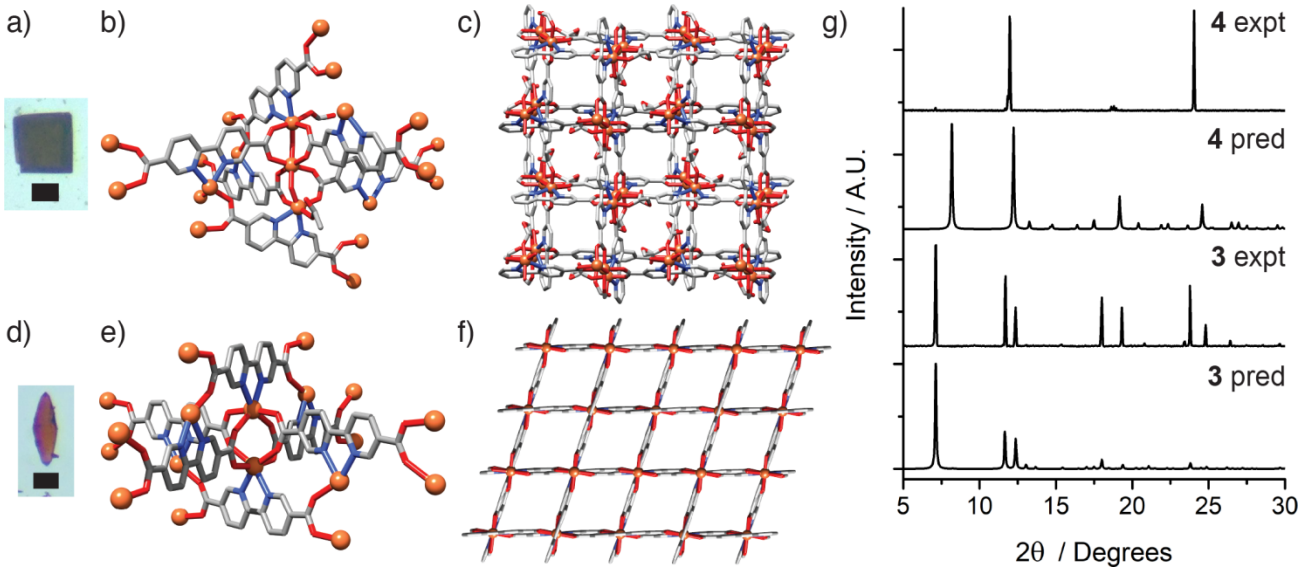

Figure 7. a) Image of a single crystal of **3**. b) Trinuclear SBU found in the crystal structure of **3**. c) Packing structure of **3** viewed down the *c* axis. d) Image of a single crystal of **4**. e) Dinuclear paddlewheel SBU found in the crystal structure of **4**. f) Packing structure of **4** viewed down the *a* axis. g) Stacked PXRD patterns of isolated samples of **3** and **4** compared to those predicted from their crystal structures. Scale bars 100 µm. C: grey; O: red; N: blue; Fe: orange spheres; H atoms and disorder removed from crystal structure images for clarity.

The carboxylate coordination results in a paddlewheel-like square grid which is overlaid by another through the bipyridyl coordination, resulting in a tetragonal net (Figure 7c) with potential porosity.

Bond valence sum (BVS) calculations gave values of 3.021 and 3.091 for Fe1 and Fe2, respectively, indicating that both are in the +3-oxidation state. The formate anion is one of the products from the hydrolysis of DMF, which is known to occur near its boiling point (153 °C). It is therefore assumed that dimethylamine is present within the pores to balance the framework charge, making the overall formula $[H_2NMe_2][Fe^{III}_3(bpydc)_2(O)_2(OAc)(HCO_2)]_n$. **3** is structurally related to two analogues containing five-coordinate Zn^{2+} centres which have bridging carboxylates (one with formate, reported as JLU-Liu4, and one with acetate) in place of the oxo-bridges,[60-61] and a mixed-metal MOF with formula $[Fe^{III}_2Co^{II}(bpydc)_2(O)_2(H_2O)_2]$ which was prepared in a similar manner using oxo-centred mixed-metal clusters.[47]

4 crystallises as orange rods (Figure 7d) in the orthorhombic Fddd space group, and consists of $Fe_2(RCO_2)_4$ paddlewheels (Figure 7e) containing one crystallographically independent iron atom (Fe1, related by a two-fold rotation axis) in a distorted octahedral geometry capped at either end by bidentate bipyridyl units. The BVS calculation for Fe1 gives a value of 2.155, which indicates that it exists in the +2 oxidation state and that the overall formula is $[Fe^{II}(bpydc)]_n$. Each SBU is linked by four dicarboxylates to form 2D layers in a diamond array, and these layers are linked together into a 3D network through the bipyridyl linkages to give diamond-shaped channels when viewed down the *a* axis (Figure 7f), similar to those in the iron terephthalate MIL-53(Fe). Isostructural variants have previously been reported for Mn^{2+} (reported as JLU-Liu11)[62] and Cd^{2+}.[63]

In both cases, rather than preserving the Fe_3O cluster by simple substitution of the acetates by bpydc, decomposition allows formation of linear clusters with chelating nitrogen groups capping each end. In the case of **4** there is also a reduction of Fe^{3+} to Fe^{2+} during synthesis, and similar results were obtained when the reaction temperature was lowered to 120 °C, suggesting the Fe_3O cluster may not be stable in the presence of chelating N donor ligands such as bpydc. Variation of the relative ratios of the linker and acetate cluster could be used to tune between these two phases, but neither could be obtained phase pure; each sample visually contained a small proportion of the other crystal form, although PXRD analysis (Figure 7g) suggested phase pure **3** and that a structural change occurs on drying **4**. A molar ratio of approximately 1:1 (cluster:linker) favoured **3**, while adjusting the ratio to 2:1 favoured **4**. The interpenetrated MIL-126 phase is not present in any of these samples, regardless of the conditions used, confirming that, as with Sc-bpydc, the linker is unable to adopt the twisted conformation necessary to favour interpenetration. The tendency for coordination to the metal by the N-donors makes formation of the MIL-88D structure more challenging than with the scandium analogue, a reflection of the relative chemical softness of Fe^{3+} compared to Sc^{3+}. Nevertheless, it is seemingly possible to produce a phase-pure sample, despite the possibility of also forming **3** and **4**, with a further reported structure $[Fe^{II}(bpydc)(H_2O)]\cdot H_2O$ previously isolated from hydrothermal synthesis with $FeCl_2$ adding to the complexity of the system;[64] some of the modulated Fe-bpydc samples do not correspond to any of these phases, suggesting new materials or decomposition products yet to be identified.

6. Synthesis of 1 using Fe^{2+} (1′)

While Fe^{3+} salts are generally used to synthesise Fe^{3+} MOFs, there are several examples where Fe^{2+} salts have been used.[65-70] It would be expected that the necessary autoxidation of Fe^{2+} to Fe^{3+} would slow the self-assembly process and therefore lead to the thermodynamic product; in this case with bpdc linkers, the interpenetrated phase. Accordingly, only MIL-126(Fe) is obtained (Figure 8a) when $FeCl_2$ is used as the Fe source (we have termed the samples **1′** to indicate the use of Fe^{2+} starting materials), even without modulator, where $FeCl_3$ gives MIL-88D(Fe) under identical conditions, where counterions have been kept consistent to avoid potential anion templation affects[71] perturbing self-assembly (SI, Section S7). An alternative possible product MOF-106, $[Fe^{II}(bpdc)(DMF)]_n$, has previously been reported from a sealed solvothermal synthesis using a DMF/propanol mixture at 120 °C,[72] but no corresponding reflections for this phase were evident in the PXRD patterns. The porosities of the **1′** samples are greater (Figure 8b) than for the equivalent samples prepared using $FeCl_3$, suggesting enhanced crystallinity and phase purity.

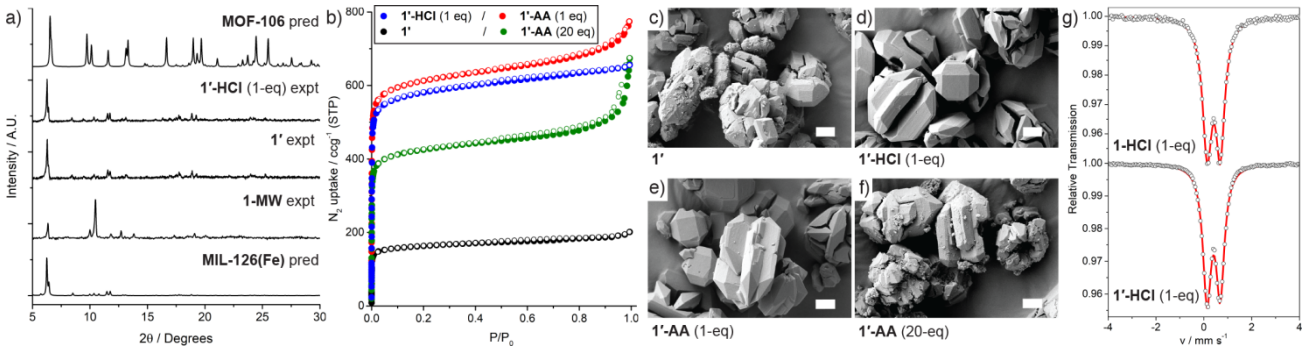

Figure 8. a) Stacked experimental PXRD patterns of **1′** and **1′-HCl** (1 eq) confirming interpenetration, compared to **1-MW** (non-interpenetrated) and predicted patterns for MIL-126(Fe) and MOF-106, $[Fe^{II}(bpdc)(DMF)]_n$ b) N_2 adsorption isotherms (77 K) for modulated samples of **1′**. Filled circles represent sorption, empty symbols desorption. SEM images of c) **1′**, d) **1′-HCl** (1 eq), e) **1′-AA** (1 eq), and f) **1′-AA** (20 eq). Scale bars 5 µm. (g) Comparison of the zero-field Mössbauer spectra of a solid samples of **1-HCl** (1 eq) (top) and **1′-HCl** (1 eq) (bottom) at 290 K. The black circles are experimental data with the fit represented by the red line.

The unmodulated sample has a relatively high nitrogen uptake, with a corresponding S_{BET} = 637 $m^2\ g^{-1}$, but use of a modulator greatly enhances the porosity. The combination of $FeCl_2$ and one equivalent of AA yielded **1′**-AA (1 eq) with S_{BET} = 2416 $m^2\ g^{-1}$, the highest value

obtained in this study and close to the predicted maximum of 2550 $m^2 g^{-1}$ for a pristine MIL-126(Fe) sample.[14] No significant hysteresis is present, even when 20 equivalents of AA are used, suggesting little or no defect induction. SEM imaging of the samples (Figures 8c-8f) shows that they are of a much higher quality than the corresponding equivalents using $FeCl_3$. The unmodulated sample **1′** and **1′-AA** (20 eq) consist of intergrown crystallites possessing distinctive crystalline faces, while **1′-AA** (1 eq) and **1′-HCl** (1 eq), consist of single crystals typical of MIL-126(Fe) as well as arrangements of intergrown crystallites. The decrease in porosity and sample quality when the concentration of AA is increased from 1 to 20 equivalents suggests that, compared to analogous synthesis using $FeCl_3$, synthesis with $FeCl_2$ requires much less modulator for optimal porosity and crystallinity.

The lack of mesoporous defects and the overall enhancement in sample quality suggest that the crystallisation process occurs differently compared to the equivalents using Fe^{3+} salts. The formation of MIL-126(Fe) indicates oxidation of Fe^{2+} to Fe^{3+}, which is a requirement for the formation of the Fe_3O clusters present in the framework. However, a mixed-valence cluster $[M^{III}{}_2M^{II}O]$ is also possible; recently this has been exploited[47] to construct MOFs with $[Fe^{III}{}_2M^{II}O(RCO_2)_6]$ SBUs. ^{57}Fe Mössbauer spectroscopy was used to investigate the Fe oxidation states; two samples were prepared in an identical manner, other than changing the iron source from Fe^{3+} to Fe^{2+}, with 1 eq of HCl as modulator to enhance sample quality while avoiding defect induction. As thermal treatment is reported to reduce Fe^{3+} to Fe^{2+} in MIL-126(Fe),[14] these samples were activated under vacuum only to accurately assess the oxidation state of the Fe in the as-synthesised form. The spectra of **1-HCl** (1 eq), prepared from $FeCl_3$, and **1′-HCl** (1 eq), prepared from $FeCl_2$, have single quadrupolar doublets and show no discernible differences (Figure 8g). The isomer shifts and quadrupolar splittings are consistent with homovalent $[Fe^{III}{}_3O(RCO_2)_6]$ SBUs for both samples when compared to data from discrete complexes[73-76] and analogous MOFs,[77] confirming complete oxidation of Fe^{2+} to Fe^{3+} in the synthesis of **1′-HCl** (1 eq).

The presence of Fe^{2+} during synthesis, which is a softer Lewis acid, may increase ligand lability, coordinative reversibility, and "error-checking", thus reducing defectivity and enhancing crystallinity in the resulting MOFs. This could explain the success of this synthetic approach and why only a relatively small amount of modulator (1 equiv of AA) is required to induce dramatic enhancements to the porosity of **1′**. A similar observation has been reported elsewhere for the iron(III) trimesate MIL-100(Fe) when synthesised using an Fe^{2+} salt, with

higher crystallinity and porosity achieved from room temperature syntheses without requiring HF.[70] These results show that tuning of the initial oxidation state of the metal – a process we term oxidation modulation – is also a potential strategy for controlling the phase purity, as well as physical properties of the resulting MOFs, by providing additional kinetic barriers during the self-assembly process.[78]

7. Conclusions

To conclude, the synthesis of MIL-126/MIL-88D type MOFs based on Fe^{3+} and bpdc and bpydc has been investigated, and controllable synthetic routes to both interpenetrated and non-interpenetrated materials have been established. When using bpdc as the linker, coordination modulation has been demonstrated to slow the self-assembly process to favour the interpenetrated MIL-126(Fe) framework as the thermodynamic product, while the non-interpenetrated framework MIL-88D(Fe) appears to be a kinetic product that can only be obtained through unmodulated synthesis at relatively low temperatures (≤120 °C). DFT simulations show a strong preference for the arrangement of capping species in MIL-126 that is not evident for MIL-88D, for both Fe^{3+} and Sc^{3+} analogues, indicating that the thermodynamics of correlated anion disorder influence the formation of MIL-126(Fe). By varying the quantity and identity of the modulator added during synthesis, it is possible to tune between these two crystal phases and also control the size, morphology, and defectivity of the interpenetrated MOF. Significantly, PXRD analysis alone is not to determine phase purity of MIL-126(Fe); SEM images show appreciable quantities of MIL-88D(Fe) in many samples which do not diffract strongly and detract from the porosity of the bulk material.

The use of bpydc in place of bpdc inhibits the formation of the interpenetrated MIL-126(Fe) phase as a consequence of the prohibitively distorted linker conformation required, as previously demonstrated for Sc^{3+} analogues, and confirmed by new DFT calculations and modulated experiments. In contrast to Sc^{3+}, Fe^{3+} can coordinate to the bipyridyl N-donors and form MOFs with different topologies to MIL-88D, which can also be isolated under specific modulation conditions. Both new structures are non-interpenetrated and possess significant potential void space, however, phase-pure samples of either MOF could not be obtained on a large enough scale for further investigation.

Finally, the use of an Fe^{2+} salt as starting material effectively slows the synthesis to favour interpenetration and, when combined with modulation, greatly enhances the porosity of the resulting MOF without inducing defectivity. The overall greater sample quality suggests that oxidation modulation – the deliberate use of metal precursors in different oxidation states to that found in the resulting MOF – could be a simple and effective synthetic tool for preparing high quality MOFs with improved physical properties crystallinity and porosity, and for discovering new phases.

8. Acknowledgements

RSF thanks the Royal Society for a University Research Fellowship. This project received funding in part from the European Research Council (ERC) under the European Union's Horizon 2020 Programme for Research and Innovation (grant agreement no. 677289, SCoTMOF, ERC-2015-STG). Via our membership of the UK's HEC Materials Chemistry Consortium, which is funded by EPSRC (EP/L000202, EP/R029431), this work used the 'ARCHER UK National Supercomputing Service (http://www.archer.ac.uk). MMK is grateful to the Deutsche Forschungsgemeinschaft (DFG Research Grant KH 279/3) and Emerging Talents Initiative (ETI) program of the FAU Erlangen-Nürnberg for financial support; Prof. Karsten Meyer (FAU Erlangen-Nürnberg) is acknowledged for providing access to Mössbauer spectrometer and his general support throughout the years; Dr. Jörg Sutter is acknowledged for measuring Mössbauer spectra.

9. Supporting Information

Synthesis of all MOFs, powder and single crystal X-ray diffraction, gas adsorption, scanning electron microscopy, thermogravimetric analysis, Mössbauer spectroscopy, DFT simulations.

10. References

1. James, S. L. Metal-organic frameworks. *Chem. Soc. Rev.* **2003**, *32* (5), 276-288.

2. Spokoyny, A. M.; Kim, D.; Sumrein, A.; Mirkin, C. A. Infinite coordination polymer nano- and microparticle structures. *Chem. Soc. Rev.* **2009**, *38* (5), 1218-1227.

3. Zhou, H.-C.; Long, J. R.; Yaghi, O. M. Introduction to Metal–Organic Frameworks. *Chem. Rev.* **2012**, *112* (2), 673-674.

4. Furukawa, H.; Cordova, K. E.; O'Keeffe, M.; Yaghi, O. M. The Chemistry and Applications of Metal-Organic Frameworks. *Science* **2013**, *341* (6149) 1230444.

5. He, Y.; Chen, F.; Li, B.; Qian, G.; Zhou, W.; Chen, B. Porous metal–organic frameworks for fuel storage. *Coord. Chem. Rev.* **2018**, *373*, 167-198.

6. Ma, S.; Zhou, H.-C. Gas storage in porous metal–organic frameworks for clean energy applications. *Chem. Commun.* **2010**, *46* (1), 44-53.

7. Lee, J.; Farha, O. K.; Roberts, J.; Scheidt, K. A.; Nguyen, S. T.; Hupp, J. T. Metal–organic framework materials as catalysts. *Chem. Soc. Rev.* **2009**, *38* (5), 1450-1459.

8. Wang, H.; Lustig, W. P.; Li, J. Sensing and capture of toxic and hazardous gases and vapors by metal–organic frameworks. *Chem. Soc. Rev.* **2018**, *47* (13), 4729-4756.

9. Lustig, W. P.; Mukherjee, S.; Rudd, N. D.; Desai, A. V.; Li, J.; Ghosh, S. K. Metal–organic frameworks: functional luminescent and photonic materials for sensing applications. *Chem. Soc. Rev.* **2017**, *46* (11), 3242-3285.

10. Xu, R.; Wang, Y.; Duan, X.; Lu, K.; Micheroni, D.; Hu, A.; Lin, W. Nanoscale Metal–Organic Frameworks for Ratiometric Oxygen Sensing in Live Cells. *J. Am. Chem. Soc.* **2016**, *138* (7), 2158-2161.

11. Horcajada, P.; Gref, R.; Baati, T.; Allan, P. K.; Maurin, G.; Couvreur, P.; Férey, G.; Morris, R. E.; Serre, C. Metal–Organic Frameworks in Biomedicine. *Chem. Rev.* **2012**, *112* (2), 1232-1268.

12. Huxford, R. C.; Della Rocca, J.; Lin, W. Metal–organic frameworks as potential drug carriers. *Curr. Opin. Chem. Biol.* **2010**, *14* (2), 262-268.

13. Surble, S.; Serre, C.; Mellot-Draznieks, C.; Millange, F.; Ferey, G. A new isoreticular class of metal-organic-frameworks with the MIL-88 topology. *Chem. Commun.* **2006**, 284-286.

14. Dan-Hardi, M.; Chevreau, H.; Devic, T.; Horcajada, P.; Maurin, G.; Férey, G.; Popov, D.; Riekel, C.; Wuttke, S.; Lavalley, J.-C.; Vimont, A.; Boudewijns, T.; de Vos, D.; Serre, C. How Interpenetration Ensures Rigidity and Permanent Porosity in a Highly Flexible Hybrid Solid. *Chem. Mater.* **2012**, *24* (13), 2486-2492.

15. Horcajada, P.; Salles, F.; Wuttke, S.; Devic, T.; Heurtaux, D.; Maurin, G.; Vimont, A.; Daturi, M.; David, O.; Magnier, E.; Stock, N.; Filinchuk, Y.; Popov, D.; Riekel, C.;

Férey, G.; Serre, C. How Linker's Modification Controls Swelling Properties of Highly Flexible Iron(III) Dicarboxylates MIL-88. *J. Am. Chem. Soc.* **2011**, *133* (44), 17839-17847.

16. Jiang, H.-L.; Makal, T. A.; Zhou, H.-C. Interpenetration control in metal–organic frameworks for functional applications. *Coord. Chem. Rev.* **2013**, *257* (15), 2232-2249.

17. Zhang, J.; Wojtas, L.; Larsen, R. W.; Eddaoudi, M.; Zaworotko, M. J. Temperature and Concentration Control over Interpenetration in a Metal−Organic Material. *J. Am. Chem. Soc.* **2009**, *131* (47), 17040-17041.

18. Yang, S.; Lin, X.; Lewis, W.; Suyetin, M.; Bichoutskaia, E.; Parker, J. E.; Tang, C. C.; Allan, D. R.; Rizkallah, P. J.; Hubberstey, P.; Champness, N. R.; Mark Thomas, K.; Blake, A. J.; Schröder, M. A partially interpenetrated metal–organic framework for selective hysteretic sorption of carbon dioxide. *Nat. Mater.* **2012**, *11* (8), 710-716.

19. Deshpande, R. K.; Waterhouse, G. I. N.; Jameson, G. B.; Telfer, S. G. Photolabile protecting groups in metal-organic frameworks: preventing interpenetration and masking functional groups. *Chem. Commun.* **2012**, *48* (10), 1574-1576.

20. Serre, C.; Mellot-Draznieks, C.; Surblé, S.; Audebrand, N.; Filinchuk, Y.; Férey, G. Role of Solvent-Host Interactions That Lead to Very Large Swelling of Hybrid Frameworks. *Science* **2007**, *315* (5820), 1828-1831.

21. Lieu, T. N.; Nguyen, K. D.; Le, D. T.; Truong, T.; Phan, N. T. S. Application of iron-based metal-organic frameworks in catalysis: oxidant-promoted formation of coumarins using $Fe_3O(BPDC)_3$ as an efficient heterogeneous catalyst. *Catal. Sci. Technol.* **2016**, *6* (15), 5916-5926.

22. Dang, H. T.; Lieu, T. N.; Truong, T.; Phan, N. T. S. Direct alkenylation of 2-substituted azaarenes with carbonyls via CH bond activation using iron-based metal-organic framework $Fe_3O(BPDC)_3$ as an efficient heterogeneous catalyst. *J. Mol. Catal. A Chem.* **2016**, *420*, 237-245.

23. Nguyen, V. T.; Ngo, H. Q.; Le, D. T.; Truong, T.; Phan, N. T. S. Iron-catalyzed domino sequences: One-pot oxidative synthesis of quinazolinones using metal–organic framework $Fe_3O(BPDC)_3$ as an efficient heterogeneous catalyst. *Chem. Eng. J.* **2016**, *284*, 778-785.

24. Horiuchi, Y.; Toyao, T.; Miyahara, K.; Zakary, L.; Van, D. D.; Kamata, Y.; Kim, T.-H.; Lee, S. W.; Matsuoka, M. Visible-light-driven photocatalytic water oxidation catalysed by iron-based metal-organic frameworks. *Chem. Commun.* **2016**, *52* (29), 5190-5193.

25. Nguyen, K. D.; Doan, S. H.; Ngo, A. N. V.; Nguyen, T. T.; Phan, N. T. S. Direct C–N coupling of azoles with ethers via oxidative C–H activation under metal–organic framework catalysis. *J. Ind. Eng. Chem.* **2016**, *44*, 136-145.

26. Giménez-Marqués, M.; Hidalgo, T.; Serre, C.; Horcajada, P. Nanostructured metal–organic frameworks and their bio-related applications. *Coord. Chem. Rev.* **2016**, *307*, 342-360.

27. Takaaki, T.; Shuhei, F.; Yohei, T.; Kaname, Y.; Seiji, I.; Susumu, K. Nanoporous Nanorods Fabricated by Coordination Modulation and Oriented Attachment Growth. *Angew. Chem. Int. Ed.* **2009**, *48* (26), 4739-4743.

28. Diring, S.; Furukawa, S.; Takashima, Y.; Tsuruoka, T.; Kitagawa, S. Controlled Multiscale Synthesis of Porous Coordination Polymer in Nano/Micro Regimes. *Chem. Mater.* **2010**, *22* (16), 4531-4538.

29. Wang, S.; McGuirk, C. M.; d'Aquino, A.; Mason Jarad, A.; Mirkin Chad, A. Metal–Organic Framework Nanoparticles. *Adv. Mater.* **2018**, *30* (37), 1800202.

30. McGuire, C. V.; Forgan, R. S. The surface chemistry of metal–organic frameworks. *Chem. Commun.* **2015**, *51* (25), 5199-5217.

31. Hermes, S.; Witte, T.; Hikov, T.; Zacher, D.; Bahnmüller, S.; Langstein, G.; Huber, K.; Fischer, R. A. Trapping Metal-Organic Framework Nanocrystals: An in-Situ Time-Resolved Light Scattering Study on the Crystal Growth of MOF-5 in Solution. *J. Am. Chem. Soc.* **2007**, *129* (17), 5324-5325.

32. Guo, H.; Zhu, Y.; Wang, S.; Su, S.; Zhou, L.; Zhang, H. Combining Coordination Modulation with Acid–Base Adjustment for the Control over Size of Metal–Organic Frameworks. *Chem. Mater.* **2012**, *24* (3), 444-450.

33. Schaate, A.; Roy, P.; Godt, A.; Lippke, J.; Waltz, F.; Wiebcke, M.; Behrens, P. Modulated Synthesis of Zr-Based Metal-Organic Frameworks: From Nano to Single Crystals. *Chem. Eur. J.* **2011**, *17* (24), 6643-6651.

34. Shuai, Y.; Liang, F.; Kecheng, W.; Jiandong, P.; Matheiu, B.; Christina, L.; Yujia, S.; Junsheng, Q.; Xinyu, Y.; Peng, Z.; Qi, W.; Lanfang, Z.; Yingmu, Z.; Liangliang, Z.; Yu, F.; Jialuo, L.; Hong-Cai, Z. Stable Metal–Organic Frameworks: Design, Synthesis, and Applications. *Adv. Mater.* **2018**, *30* (37), 1704303.

35. Devic, T.; Serre, C. High valence 3p and transition metal based MOFs. *Chem. Soc. Rev.* **2014**, *43* (16), 6097-6115.

36. Tamames-Tabar, C.; Cunha, D.; Imbuluzqueta, E.; Ragon, F.; Serre, C.; Blanco-Prieto, M. J.; Horcajada, P. Cytotoxicity of nanoscaled metal-organic frameworks. *J. Mater. Chem. B* **2014**, *2* (3), 262-271.

37. Horcajada, P.; Chalati, T.; Serre, C.; Gillet, B.; Sebrie, C.; Baati, T.; Eubank, J. F.; Heurtaux, D.; Clayette, P.; Kreuz, C.; Chang, J.-S.; Hwang, Y. K.; Marsaud, V.; Bories, P.-N.; Cynober, L.; Gil, S.; Ferey, G.; Couvreur, P.; Gref, R. Porous metal-organic-framework nanoscale carriers as a potential platform for drug delivery and imaging. *Nat. Mater.* **2010**, *9* (2), 172-178.

38. Marshall, R. J.; Lennon, C. T.; Tao, A.; Senn, H. M.; Wilson, C.; Fairen-Jimenez, D.; Forgan, R. S. Controlling interpenetration through linker conformation in the modulated synthesis of Sc metal-organic frameworks. *J. Mater. Chem. A* **2018**, *6* (3), 1181-1187.

39. Pham, M.-H.; Vuong, G.-T.; Vu, A.-T.; Do, T.-O. Novel Route to Size-Controlled Fe–MIL-88B–NH_2 Metal–Organic Framework Nanocrystals. *Langmuir* **2011**, *27* (24), 15261-15267.

40. Liu, Y.; Gao, P.; Huang, C.; Li, Y. Shape- and size-dependent catalysis activities of iron-terephthalic acid metal-organic frameworks. *Sci. China Chem.* **2015**, *58* (10), 1553-1560.

41. Bagherzadeh, E.; Zebarjad, S. M.; Madaah, H. H. R. Morphology Modification of Iron Fumarate MIL-88A Metal-Organic Framework Using Formic acid and Acetic Acid as Modulators. *Eur. J. Inorg. Chem.* **2018**, *2018* (18), 1905-1915.

42. Deleu, W. P. R.; Rivero, G.; Teixeira, R. F. A.; Du Prez, F. E.; De Vos, D. E. Metal–Organic Frameworks Encapsulated in Photocleavable Capsules for UV-Light Triggered Catalysis. *Chem. Mater.* **2015**, *27* (16), 5495-5502.

43. Mejia-Ariza, R.; Huskens, J. The effect of PEG length on the size and guest uptake of PEG-capped MIL-88A particles. *J. Mater. Chem. B* **2016**, *4* (6), 1108-1115.

44. Bagherzadeh, E.; Zebarjad, S. M.; Madaah Hosseini, H. R.; Chagnon, P. Preparation, Optimization and Evolution of the Kinetic Mechanism of Fe-MIL-88A Metal-Organic Framework. *CrystEngComm* **2019**, *21* (3), 544-553.

45. Feng, D.; Wang, K.; Wei, Z.; Chen, Y.-P.; Simon, C. M.; Arvapally, R. K.; Martin, R. L.; Bosch, M.; Liu, T.-F.; Fordham, S.; Yuan, D.; Omary, M. A.; Haranczyk, M.; Smit, B.; Zhou, H.-C. Kinetically tuned dimensional augmentation as a versatile synthetic route towards robust metal–organic frameworks. *Nat. Commun.* **2014**, *5*, 5723.

46. Timon, R.; Raquel, M.-A.; M., E. R. J.; Wies, v. R.; Jurriaan, H. Metal–Organic Frameworks (MOFs) as Multivalent Materials: Size Control and Surface Functionalization by Monovalent Capping Ligands. *Chem. Eur. J.* **2015**, *21* (29), 10296-10301.

47. Peng, L.; Asgari, M.; Mieville, P.; Schouwink, P.; Bulut, S.; Sun, D. T.; Zhou, Z.; Pattison, P.; van Beek, W.; Queen, W. L. Using Predefined $M_3(\mu_3\text{-O})$ Clusters as Building Blocks for an Isostructural Series of Metal–Organic Frameworks. *ACS Appl. Mater. Interfaces* **2017**, *9* (28), 23957-23966.

48. Helm, L.; Merbach, A. E. Inorganic and Bioinorganic Solvent Exchange Mechanisms. *Chem. Rev.* **2005**, *105* (6), 1923-1960.

49. Toby, B. H.; Von Dreele, R. B. GSAS-II: the genesis of a modern open-source all purpose crystallography software package. *J. Appl. Cryst.* **2013**, *46(2)*, 544-549.

50. Keen, D. A.; Goodwin, A. L. The crystallography of correlated disorder. *Nature* **2015**, *521*, 303.

51. Morris, W.; Wang, S.; Cho, D.; Auyeung, E.; Li, P.; Farha, O. K.; Mirkin, C. A. Role of Modulators in Controlling the Colloidal Stability and Polydispersity of the UiO-66 Metal–Organic Framework. *ACS Appl. Mater. Interfaces* **2017**, *9* (39), 33413-33418.

52. Sawano, T.; Thacker, N. C.; Lin, Z.; McIsaac, A. R.; Lin, W. Robust, Chiral, and Porous BINAP-Based Metal–Organic Frameworks for Highly Enantioselective Cyclization Reactions. *J. Am. Chem. Soc.* **2015**, *137* (38), 12241-12248.

53. Shearer, G. C.; Chavan, S.; Bordiga, S.; Svelle, S.; Olsbye, U.; Lillerud, K. P. Defect Engineering: Tuning the Porosity and Composition of the Metal–Organic Framework UiO-66 via Modulated Synthesis. *Chem. Mater.* **2016**, *28* (11), 3749-3761.

54. Yuan, S.; Zou, L.; Li, H.; Chen, Y.-P.; Qin, J.; Zhang, Q.; Lu, W.; Hall, M. B.; Zhou, H.-C. Flexible Zirconium Metal-Organic Frameworks as Bioinspired Switchable Catalysts. *Angew. Chem. Int. Ed.* **2016**, *55* (36), 10776-10780.

55. Abánades Lázaro, I.; Abánades Lázaro, S.; Forgan, R. S. Enhancing anticancer cytotoxicity through bimodal drug delivery from ultrasmall Zr MOF nanoparticles. *Chem. Commun.* **2018**, *54* (22), 2792-2795.

56. Abánades Lázaro, I.; Haddad, S.; Sacca, S.; Orellana-Tavra, C.; Fairen-Jimenez, D.; Forgan, R. S. Selective Surface PEGylation of UiO-66 Nanoparticles for Enhanced Stability, Cell Uptake, and pH-Responsive Drug Delivery. *Chem* **2017**, *2* (4), 561-578.

57. Marshall, R. J.; Hobday, C. L.; Murphie, C. F.; Griffin, S. L.; Morrison, C. A.; Moggach, S. A.; Forgan, R. S. Amino acids as highly efficient modulators for single crystals

of zirconium and hafnium metal-organic frameworks. *J. Mater. Chem. A* **2016**, *4* (18), 6955-6963.

58. Bosch, M.; Yuan, S.; Rutledge, W.; Zhou, H.-C. Stepwise Synthesis of Metal–Organic Frameworks. *Acc. Chem. Res.* **2017**, *50* (4), 857-865.

59. Katz, M. J.; Brown, Z. J.; Colón, Y. J.; Siu, P. W.; Scheidt, K. A.; Snurr, R. Q.; Hupp, J. T.; Farha, O. K. A facile synthesis of UiO-66, UiO-67 and their derivatives. *Chem. Commun.* **2013**, *49* (82), 9449-9451.

60. Wang, J.; Luo, J.; Zhao, J.; Li, D.-S.; Li, G.; Huo, Q.; Liu, Y. Assembly of Two Flexible Metal–Organic Frameworks with Stepwise Gas Adsorption and Highly Selective CO_2 Adsorption. *Cryst. Growth Des.* **2014**, *14* (5), 2375-2380.

61. Bon, V.; Kavoosi, N.; Senkovska, I.; Müller, P.; Schaber, J.; Wallacher, D.; Többens, D. M.; Mueller, U.; Kaskel, S. Tuning the flexibility in MOFs by SBU functionalization. *Dalton Trans.* **2016**, *45* (10), 4407-4415.

62. Wang, J.; Jing, X.; Cao, Y.; Li, G.; Huo, Q.; Liu, Y. Structural diversity and magnetic properties of three metal–organic frameworks assembled from a T-shaped linker. *CrystEngComm* **2015**, *17* (3), 604-611.

63. Liu, Y. CCDC 927168: Experimental Crystal Structure Determination, **2016**, DOI: 10.5517/ccdc.csd.cc103snk.

64. Finn, R. C.; Zubieta, J. Hydrothermal synthesis and structural characterization of the two-dimensional networks $[M(H_2O)(bpy\text{-}dicarb)]\cdot H_2O$ (M=Fe, Co, Ni, Zn; bpy-dicarb=2,2′-bipyridyl-4,4′-dicarboxylic acid). *Solid State Sci.* **2002**, *4* (1), 83-86.

65. Choi, S. B.; Seo, M. J.; Cho, M.; Kim, Y.; Jin, M. K.; Jung, D.-Y.; Choi, J.-S.; Ahn, W.-S.; Rowsell, J. L. C.; Kim, J. A Porous and Interpenetrated Metal–Organic Framework Comprising Tetranuclear Iron^{III}–Oxo Clusters and Tripodal Organic Carboxylates and Its Implications for (3,8)-Coordinated Networks. *Cryst. Growth Des.* **2007**, *7* (11), 2290-2293.

66. Cairns, A. J.; Eckert, J.; Wojtas, L.; Thommes, M.; Wallacher, D.; Georgiev, P. A.; Forster, P. M.; Belmabkhout, Y.; Ollivier, J.; Eddaoudi, M. Gaining Insights on the H_2–Sorbent Interactions: Robust soc-MOF Platform as a Case Study. *Chem. Mater.* **2016**, *28* (20), 7353-7361.

67. Yoon, J. H.; Choi, S. B.; Oh, Y. J.; Seo, M. J.; Jhon, Y. H.; Lee, T.-B.; Kim, D.; Choi, S. H.; Kim, J. A porous mixed-valent iron MOF exhibiting the acs net: Synthesis, characterization and sorption behavior of $Fe_3O(F_4BDC)_3(H_2O)_3\cdot(DMF)_{3.5}$. *Catal. Today* **2007**, *120* (3), 324-329.

68. Sanselme, M.; Grenèche, J.-M.; Riou-Cavellec, M.; Férey, G. The first ferric carboxylate with a three-dimensional hydrid open-framework (MIL-82): its synthesis, structure, magnetic behavior and study of its dehydration by Mössbauer spectroscopy. *Solid State Sci.* **2004**, *6* (8), 853-858.

69. Sudik, A. C.; Côté, A. P.; Yaghi, O. M. Metal-Organic Frameworks Based on Trigonal Prismatic Building Blocks and the New "acs" Topology. *Inorg. Chem.* **2005**, *44* (9), 2998-3000.

70. Guesh, K.; Caiuby, C. A. D.; Mayoral, Á.; Díaz-García, M.; Díaz, I.; Sanchez-Sanchez, M. Sustainable Preparation of MIL-100(Fe) and Its Photocatalytic Behavior in the Degradation of Methyl Orange in Water. *Cryst. Growth Des.* **2017**, *17* (4), 1806-1813.

71. Vuong, G.-T.; Pham, M.-H.; Do, T.-O. Direct synthesis and mechanism of the formation of mixed metal Fe_2Ni-MIL-88B. *CrystEngComm* **2013**, *15* (45), 9694-9703.

72. Eddaoudi, M.; Kim, J.; Vodak, D.; Sudik, A.; Wachter, J.; O'Keeffe, M.; Yaghi, O. M. Geometric requirements and examples of important structures in the assembly of square building blocks. *Proc. Natl. Acad. Sci. U.S.A.* **2002**, *99* (8), 4900-4904.

73. Dziobkowski, C. T.; Wrobleski, J. T.; Brown, D. B. Magnetic properties and Moessbauer spectra of several iron(III)-dicarboxylic acid complexes. *Inorg. Chem.* **1981**, *20* (3), 671-678.

74. Oh, S. M.; Kambara, T.; Hendrickson, D. N.; Sorai, M.; Kaji, K.; Woehler, S. E.; Wittebort, R. J. Phase transitions affecting intramolecular electron transfer in mixed-valence trinuclear iron acetate complexes. *J. Am. Chem. Soc.* **1985**, *107* (19), 5540-5541.

75. Sato, T.; Ambe, F.; Endo, K.; Katada, M.; Maeda, H.; Nakamoto, T.; Sano, H. Mixed-Valence States of $[Fe_3O(CH_2XCO_2)_6(H_2O)_3]\cdot nH_2O$ (X = H, Cl, and Br) Characterized by X-ray Crystallography and ^{57}Fe-Mössbauer Spectroscopy. *J. Am. Chem. Soc.* **1996**, *118* (14), 3450-3458.

76. Fernandes, C.; Stadler, E.; Drago, V.; Jorge da Cunha, C.; Hiroko Kuwabara, I. Mössbauer, vibrational and electronic spectroscopy of trinuclear μ-oxo iron(III) acetate clusters with pyridine and derivatives as ligands. *Spectrochim. Acta A* **1996**, *52* (14), 1815-1821.

77. Ma, M.; Noei, H.; Mienert, B.; Niesel, J.; Bill, E.; Muhler, M.; Fischer, R. A.; Wang, Y.; Schatzschneider, U.; Metzler-Nolte, N. Iron Metal–Organic Frameworks MIL-88B and NH_2-MIL-88B for the Loading and Delivery of the Gasotransmitter Carbon Monoxide. *Chem. Eur. J.* **2013**, *19* (21), 6785-6790.

78. Bosch, M.; Sun, X.; Yuan, S.; Chen, Y.-P.; Wang, Q.; Wang, X.; Zhou, H.-C. Modulated Synthesis of Metal-Organic Frameworks through Tuning of the Initial Oxidation State of the Metal. *Eur. J. Inorg. Chem.* **2016**, *2016* (27), 4368-4372.

11. Table of Contents Image

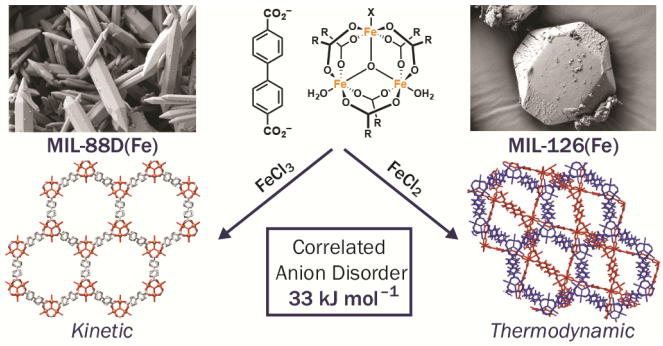

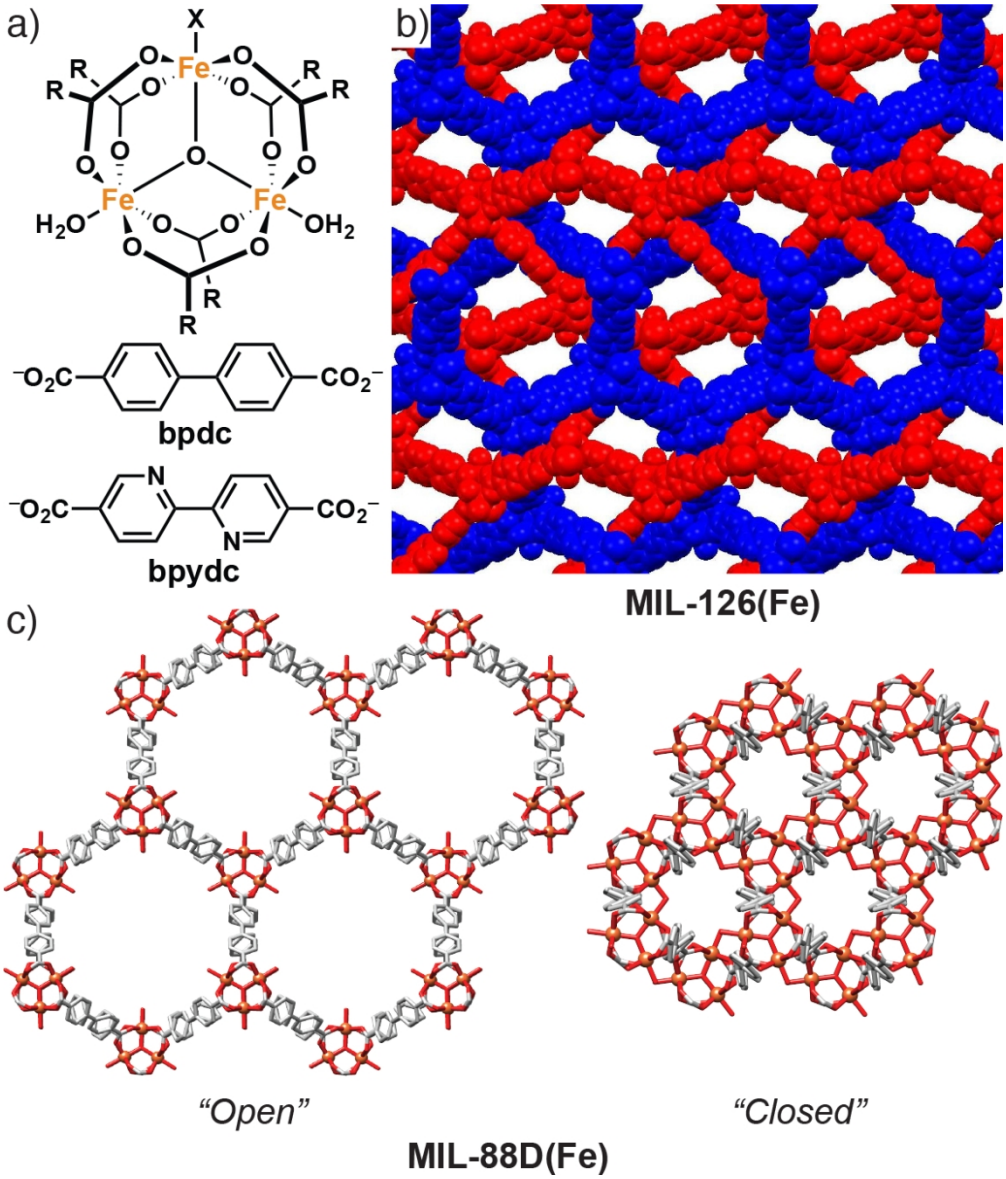

Fig 1 single column

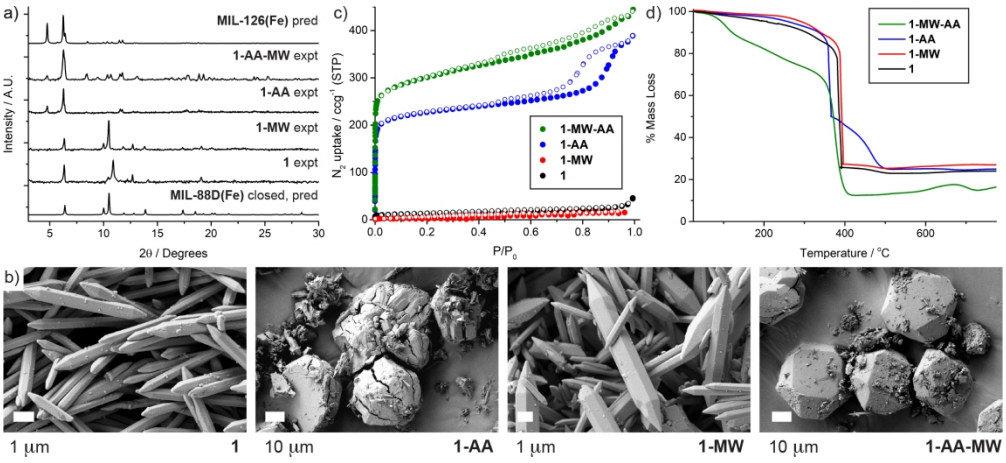

Fig 2 double column

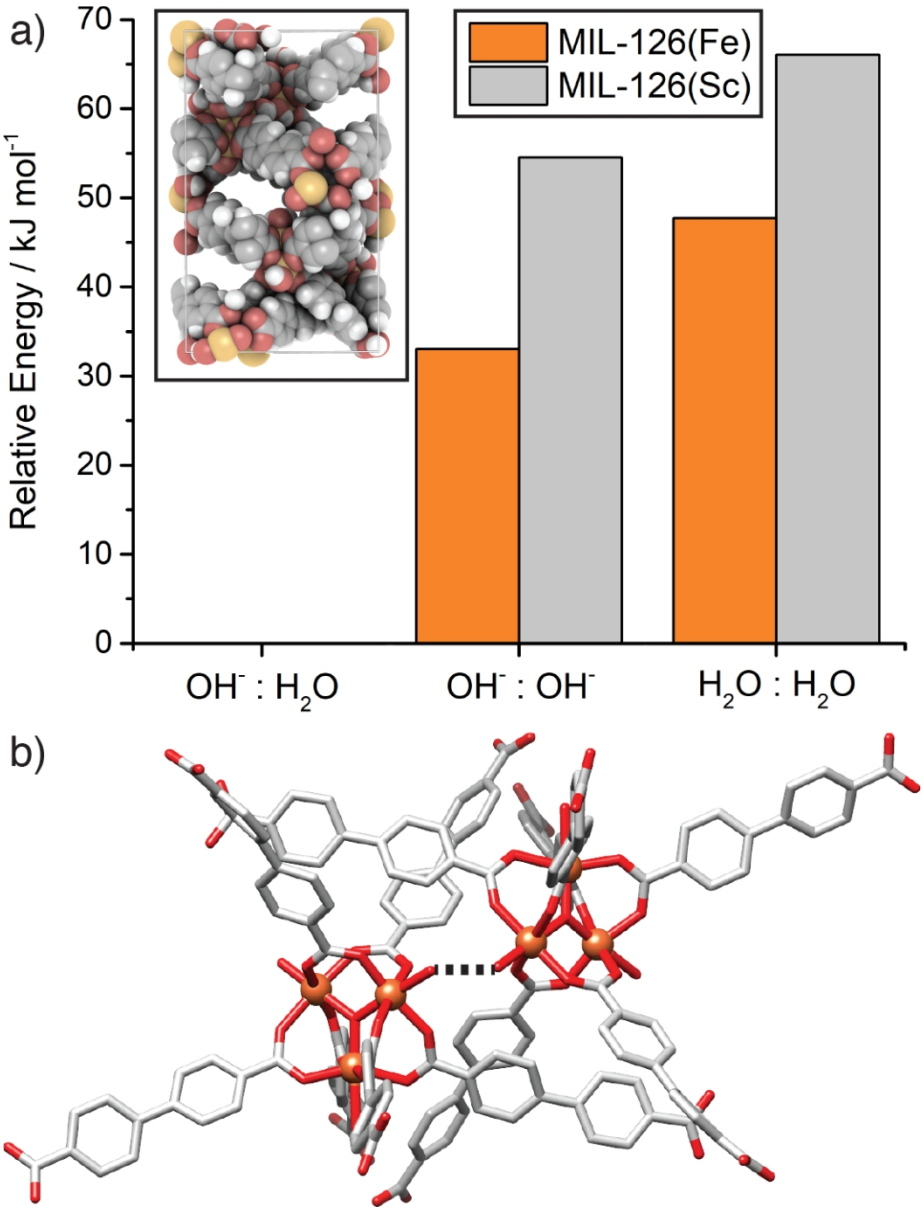

Fig 3 single column

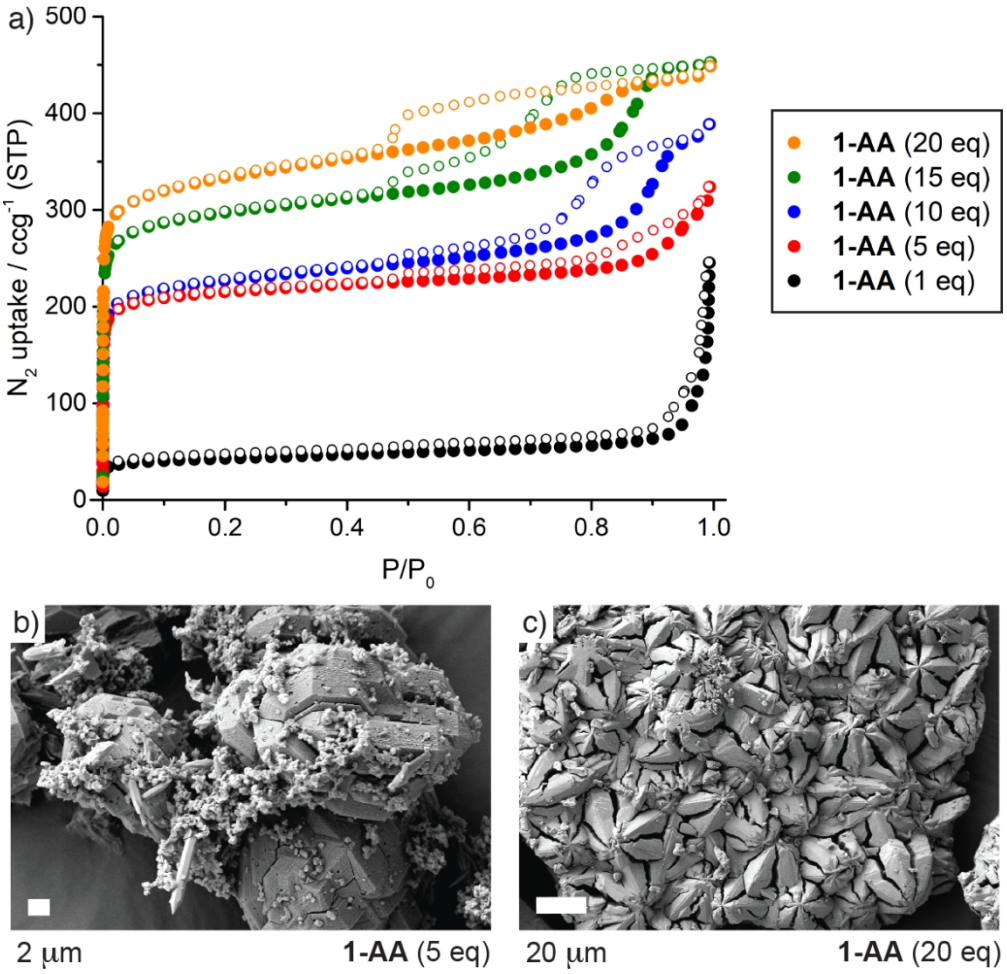

Fig 4 single column

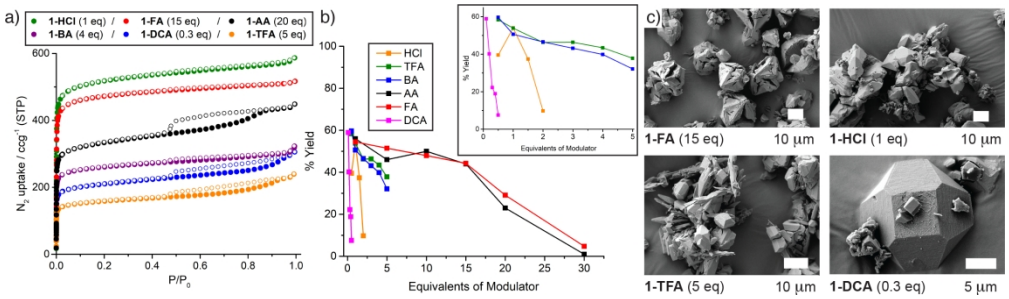

Fig 5 double column

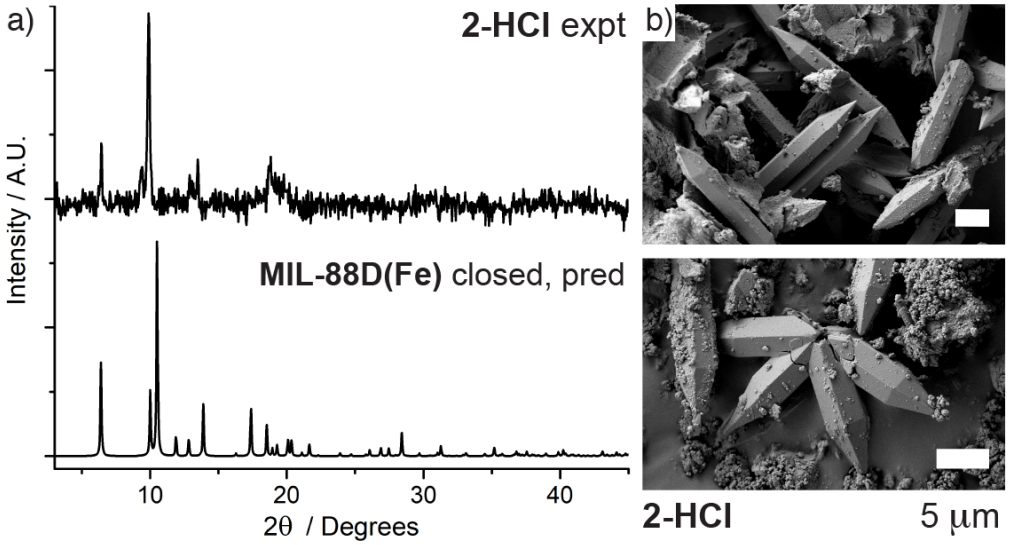

Fig 6 single cloumn

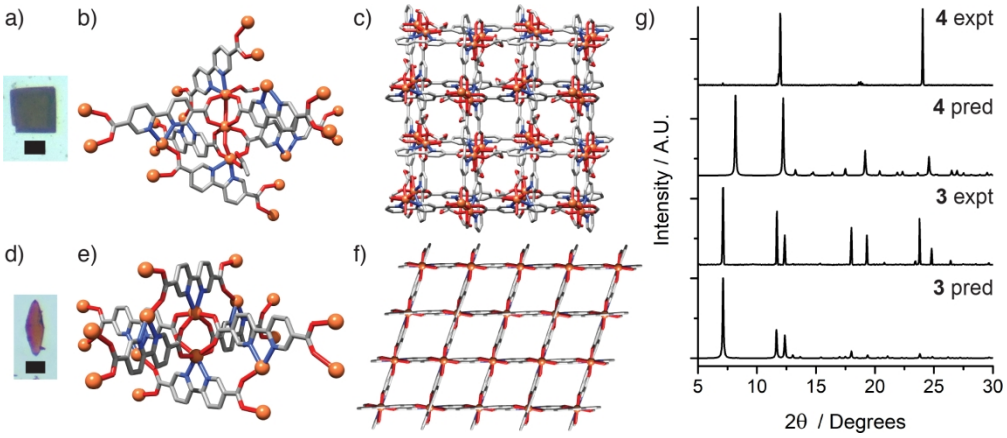

Figure 7 double column

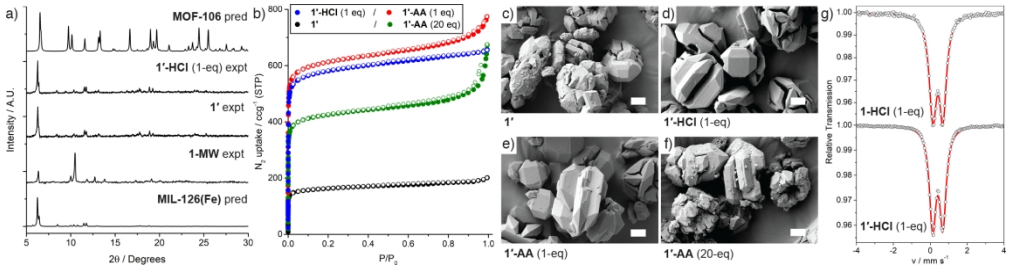

Figure 8 double column

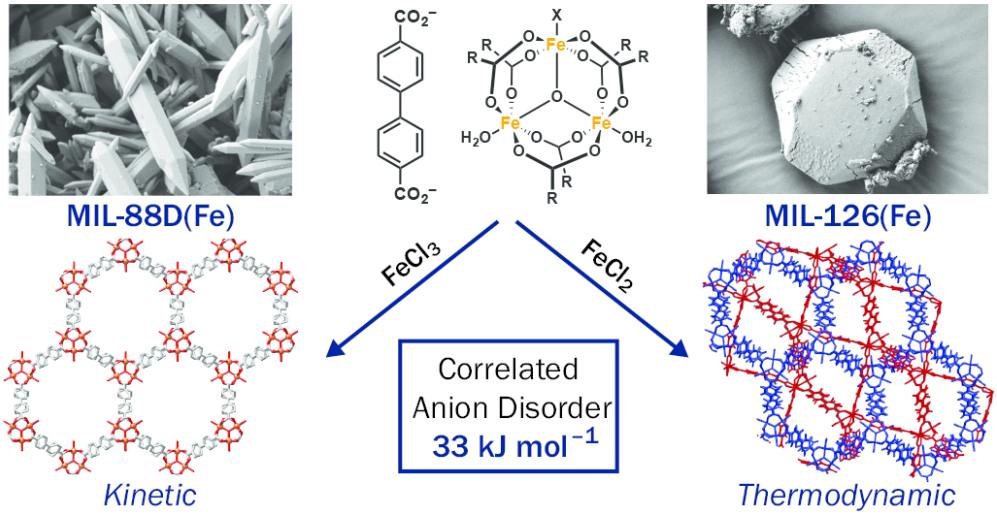
MIL-88D(Fe)
MIL-126(Fe)
FeCl3
FeCl2
Correlated
Anion Disorder
33 kJ mol−1
Kinetic
Thermodynamic